IL NUOVO CIMENTO **40 C** (2017) 89
DOI 10.1393/ncc/i2017-17089-2

COMMUNICATIONS: SIF Congress 2016

Numerical investigation of tearing modes amplitude oscillations

A. CASOLARI([1])(*) on behalf of G. PUCELLA([2])

([1]) *Dipartimento di Fisica Enrico Fermi, Università di Pisa - Largo Bruno Pontecorvo 3, I-56127 Pisa, Italy*
([2]) *ENEA, FSN-Fusion Physics Division, C. R. Frascati - Via E. Fermi 45, 00044 Frascati (Roma), Italy*

received 15 February 2017

Summary. — A recently observed phenomenon involving magnetic islands in high-density pulses in the Frascati Tokamak Upgrade is investigated using numerical simulations in slab geometry. This phenomenon was given the name "limit cycles" because of the figure drawn by the trajectory of the system in the amplitude/frequency plane of magnetic islands. In this regime of propagation, the magnetic islands show a quasi-periodic modulation of their amplitude and rotation frequency. The Fourier analysis of the experimental signals shows a large harmonic content, which we ascribed to a significant island deformation in the cycle phase. We performed a series of numerical simulations by integrating a four-field system of equations through a finite difference code to check this hypothesis. The results of the simulations show that a large density gradient causes a significant island deformation in the nonlinear regime, in agreement with our hypothesis. This deformation is caused by the diamagnetic velocity shear resulting from the nonlinear flattening of the density profile inside the island separatrix.

1. – Introduction

Tearing modes play a key role in magnetically confined plasmas for thermonuclear interest. The nonlinear growth of these modes leads to the formation of the so-called magnetic islands. Magnetic islands are an important issue because they cause an increased radial heat and particle transport, thus compromising confinement, and they may also lead to major disruptions. In the linear phase, magnetic islands grow as a consequence of the tearing mode instability [1]. As soon as their width becomes larger than the linear resistive layer, the nonlinear effects become dominant on the plasma inertia [2], the current becomes approximately a flux function $J(\psi)$ and the temporal

(*) ENEA guest

growth changes from exponential to algebraic. An extension of the tearing mode to finite pressure gradient is the drift-tearing mode [3]. In the presence of an equilibrium density or temperature gradient, the tearing mode acquires an oscillation frequency close to the electron drift frequency and the growth rate is significantly reduced. Many factors affect the linear stability and the mode structure of the drift-tearing mode. As stressed in [4], in the drift-tearing mode, with resistivity as the only dissipative effect, the unstable solutions are non-localized and they exist only in the form of traveling waves. However, any additional dissipative effect, such as viscosity or diffusivity, causes the mode to become localized. In the semi-collisional regime, instead, the mode becomes localized even without additional dissipative effects because of the finite ion-acoustic radius. As we will see below, this is the case of the typical experimental regimes we investigated.

The paper is organized as follows: in sect. **2** we introduce the phenomenon of "limit cycles" we attempted to reproduce in the simulations; in sect. **3** we illustrate the model equations we integrated numerically; in sect. **4** we describe the code we used and the benchmarking we performed in the case of small-density-gradient; in sect. **5** the results of our simulations in the case of large-density-gradient are displayed; conclusions are drawn in sect. **6**.

2. – Experimental observations of "limit cycle" tearing mode dynamics

Recent experimental observations on Frascati Tokamak Upgrade (FTU) have shown the existence of a new regime of propagation of magnetic islands, characterized by a quasi-periodic modulation of their amplitude and rotation frequency, which was given the name "limit cycles" [5]. The name limit cycles comes from the shape of the phase portrait of the system on the amplitude/frequency plane. The modes observed in these series of experiments are characterized by the poloidal and toroidal mode numbers $m = 2$ and $n = 1$, respectively. The presence of a phase difference between amplitude and frequency modulations causes the phase portrait to resemble a closed cycle.

Large magnetic islands appear in FTU when the plasma density is either extremely low or extremely high (close to the disruptive density limit [6]). Limit cycles are observed in the second case, whereas amplitude and frequency evolution is smooth in the first case. Measured magnetic field oscillations in low-density pulses have lower frequency and remarkably higher amplitude than in high-density pulses. Pulses featuring "limit cycles" are characterized by large temperature and density gradients around the $q = m/n = 2$ rational surface. The occurrence of these large gradients gives rise to large values of the diamagnetic frequency ω_*, which exceeds the characteristic resistive growth rate. The collisionality regime is intermediate between collisional and semicollisional [7], the ratio between resistive layer width and ion-acoustic radius being of order unity. The typical island width (1–2 cm) is well above the characteristic size for non linear density flattening by collisional parallel transport and by the action of ion-acoustic waves [8]. In fig. 1 we show the signals corresponding to the "limit cycle" activity during pulse #34843 in FTU (figures taken from [5] with permission of the authors). The five panels in the left figure show, from top to bottom: the electron density, the time derivative of the instantaneous poloidal magnetic field, the instantaneous poloidal magnetic field, the envelope of the signal above (amplitude in a.u.) and the oscillation frequency. The right figure shows a single period of the amplitude and frequency oscillations taken from the same pulse. Furthermore, the Fourier analysis of the experimental signals (not displayed here) shows a large harmonic content, in particular in the decreasing phase of the cycle, which we ascribed to a significant island deformation. We attributed this deformation to the shear

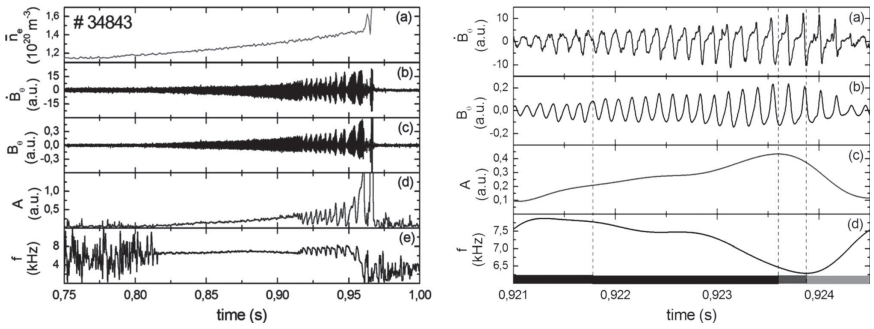

Fig. 1. – Left figure, from top to bottom: electron density, time derivative of the instantaneous poloidal magnetic field, instantaneous poloidal magnetic field, envelope of the signal above (amplitude in a.u.) and oscillation frequency. Right figure: same quantities as above for a single period of the amplitude and frequency oscillation. Figures taken from [5] with permission of the authors.

in the diamagnetic drift velocity which arises in the nonlinear regime when the density profile becomes flat inside the separatrix because of the action of the ion-acoustic waves, which is expected to become significant when the island width W becomes larger than the ion-acoustic radius ρ_s times L_s/L_n [9], or by the collisional parallel transport, which is the dominant mechanism in the semi-collisional regime [8].

3. – Modified four-field model

Here we present the system of equations we integrated numerically to explore the time evolution of the fields close to a magnetic island. This model includes the effects of finite ion-acoustic radius ρ_s, the finite-β effects, the diamagnetic drift frequency ω_* and the nonlinear flattening of the density profile inside the separatrix. The starting equations are

$$\begin{aligned} &\boldsymbol{E} + \boldsymbol{V}_e \wedge \boldsymbol{B} + \frac{\nabla P_e}{e n_0} = \eta \boldsymbol{J}, \\ &\frac{\partial n}{\partial t} + \boldsymbol{V} \cdot \nabla n + n \nabla \cdot \boldsymbol{V} = 0, \\ &m_i n_0 \left(\frac{\partial \boldsymbol{V}}{\partial t} + \boldsymbol{V} \cdot \nabla \boldsymbol{V} \right) = \boldsymbol{J} \wedge \boldsymbol{B} - \nabla P. \end{aligned} \tag{1}$$

The first of eqs. (1) is Ohm's law, corresponding to the electron momentum equation without the electron inertia. The second one is the continuity equation, the third one is the sum of the ion and electron momentum equations. The fourth equation we need is the vorticity equation, which comes from taking the curl of the momentum equation. We assume the following form for the electromagnetic fields:

$$\begin{aligned} &\boldsymbol{E}_\parallel = -\nabla_\parallel \phi - \hat{e}_z \partial_t \psi, \\ &\boldsymbol{B} = \hat{e}_z B_0 + \nabla \psi \wedge \hat{e}_z; \end{aligned} \tag{2}$$

Equations (1) are successively reduced in order to remove the fast dynamics associated with the fast magneto-acoustic waves [10] and then turned dimensionless by choosing an

appropriate normalization for the fields. $V_{\parallel e}$ can be expressed in terms of $V_{\parallel i}$ by using the definition of the parallel current $J_\parallel = ne(V_{\parallel i} - V_{\parallel e})$. The four fields we are going to use are the magnetic flux function ψ, the density n, the electrostatic potential ϕ and the parallel ion velocity V. The current $J_\parallel$ is determined by Ampere's law. We choose to normalize the time-derivative to the Alfvén time τ_A and the radial distance x to the shear length L_s. The normalization of the fields is shown below:

$$
\begin{aligned}
&\hat{\psi} = \frac{A_\parallel}{B_0 L_s}, \quad \hat{\phi} = \frac{\phi}{B_0 v_A L_s}, \quad \hat{n} = \frac{n}{n_0}\frac{L_n}{L_s}, \quad \hat{J}_\parallel = J_\parallel \frac{\mu_0 L_s}{B_0}, \\
&\hat{V}_\parallel = \frac{V_\parallel}{v_A}\frac{L_s}{L_n}, \quad \hat{\eta} = \eta \frac{\tau_A}{\mu_0 L_s^2}, \quad \partial_{\hat{t}} = \tau_A \partial_t, \quad \partial_{\hat{x}} = L_s \partial_x, \quad \partial_{\hat{y}} = \partial_y / k_\theta,
\end{aligned}
\tag{3}
$$

where $k_y v_A = \tau_A^{-1}$ and k_y is the poloidal wavenumber (equivalent to m/r_s in cylindrical geometry). By using the normalization eqs. (3), our four-field system becomes

$$
\begin{aligned}
&\frac{\partial \hat{\psi}}{\partial \hat{t}} + \left[\hat{\phi} - \frac{\beta}{2}\frac{\delta_i}{L_n}\hat{n}, \hat{\psi}\right] + \hat{\eta}\hat{J}_\parallel = 0, \\
&\frac{\partial \hat{n}}{\partial \hat{t}} + \left[\hat{\phi}, \hat{n}\right] + \left(\frac{L_n}{L_s}\right)^2 \left[\hat{V}_\parallel + \frac{\delta_i}{L_n}\hat{J}_\parallel, \hat{\psi}\right] = 0, \\
&\frac{\partial \hat{V}_\parallel}{\partial \hat{t}} + [\hat{\phi}, \hat{V}_\parallel] + \left(\frac{L_s}{L_n}\right)^2 \frac{\beta}{2}(1+\tau)[\hat{n}, \hat{\psi}] = 0, \\
&\frac{\partial}{\partial \hat{t}}\hat{\nabla}^2\hat{\phi} + \partial_{\hat{x}}\left[\hat{\phi} + \tau\frac{\beta}{2}\frac{\delta_i}{L_n}\hat{n}, \partial_{\hat{x}}\hat{\phi}\right] + [\hat{J}_\parallel, \hat{\psi}] = 0.
\end{aligned}
\tag{4}
$$

In the equations above, $\beta/2 = c_s^2/v_A^2$, $c_s^2 = T_e/m_i$ is the ion-acoustic velocity and $\delta_i = \omega_{pi}/c$ is the ion inertial skin length.

4. – Implementation and benchmark of the code

In our simulations, we chose a Harris equilibrium [11] $B(x) = B_0 \tanh(x)$, whose linear stability parameter, normalized to the poloidal wavenumber k_y, is [12]

$$
\Delta' = 2\left(\frac{1}{k} - k\right); \tag{5}
$$

Equations (4) have been integrated numerically by splitting all the fields in two parts: an equilibrium, independent of time, and an evolving perturbation. The perturbed component is advanced in time by an explicit, fourth order Adam-Bashforth scheme. The equations are solved in a 2D-slab geometry, with periodic boundary conditions along the y-direction. Dirichlet conditions are applied at the edges of the x-axis, imposing that all the perturbed fields go to zero. The integration box is defined by $-L_x < x < L_x$ and $-L_y < y < L_y$, where $k = 1/L_y$ is imposed. L_x must be chosen large enough to allow the fields to go smoothly to zero. The choice of L_y instead determines the linear mode instability through the stability parameter Δ' [13].

To begin with, we performed a series of numerical integrations in the case of a small density gradient. We integrated eqs. (4) by choosing a set of parameters such that the

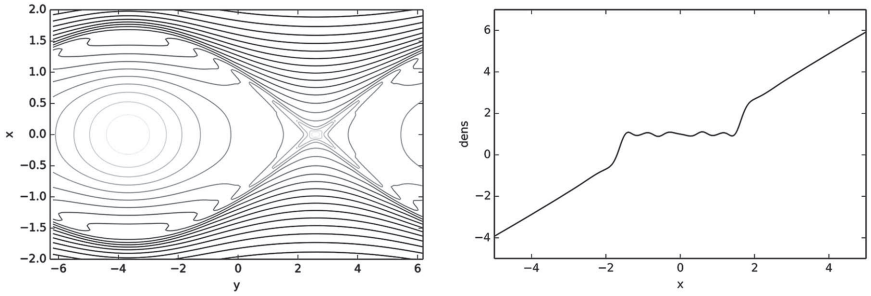

Fig. 2. – Contour curves of the current J (left) and radial profile of the density across the O-point (right) in the nonlinear regime of the drift-tearing mode for the choice $\Delta' = 3$ and $\beta = 0.05$.

diamagnetic effects do not modify significantly the nonlinear island dynamics and consistent with the simulations performed in [4]. The normalization chosen in the paper above introduces the parameter ρ, corresponding to the ion-acoustic radius ρ_s normalized to the gradients length scale L. The relation between the parameters entering our equations and the quantities ρ and ω_* is provided below:

$$\omega_* = \frac{\beta}{2}\frac{\delta_i}{L_n}, \qquad \rho^2 = \frac{\beta}{2}\frac{\delta_i^2}{L_s^2}. \tag{6}$$

First we checked the linear growth rates, as determined by the logarithmic time-derivative of the magnetic flux function ψ in the X-point of the island. By computing this quantity as the slope of $\log|\psi|$, we found the growth rate $\gamma = \mathrm{d}\log|\psi|/\mathrm{d}t \approx 0.0003$. This value is in good agreement with that obtained by using the analytical expression for the growth rate eq. (7) below, with the following choice of the parameters: $\omega_* = 0.0031$, $\rho = 0.02$, $L_n = L_s = 1$, $\beta = 0.05$ and $\delta_i = 0.13$. To be consistent with [4], the simulations relative to the case above were performed with $\Delta' = 0.41$. Note that, with this choice for the parameters, we are in the so-called semi-collisional regime [4, 7]. In the semi-collisional regime, the ion-acoustic radius is larger than the linear resistive layer and the small-Δ' condition holds, which authorizes the constant-ψ approximation. In this regime, the following expression for the linear growth rate holds [4]:

$$\gamma \sim \frac{\sqrt{2}}{2\pi}\Delta'\frac{\rho\eta^{1/2}}{\omega_*^{1/2}}. \tag{7}$$

To check the behavior of the drift-tearing mode in the nonlinear regime, we chose to increase the Δ' parameter to $\Delta' = 3$, leading to a much more rapid growth, while still verifying the conditions mentioned above. In fig. 2 we show on the left the contour curves of the current J, which is nearly a flux function, and on the right the radial profile of the density across the O-point of the island. A partial flattening of the density profile occurs inside the island separatrix, which is larger at the O-point. This flattening is caused either by the action of the ion-acoustic waves, or by the collisional parallel transport, as mentioned above.

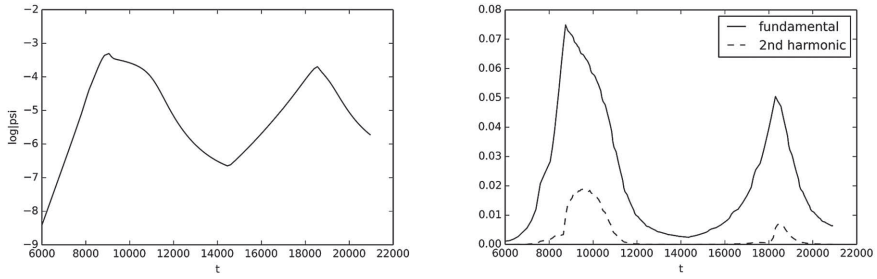

Fig. 3. – Logarithm of $|\psi|$ during the reversal of the island growth (left) and harmonic content (right) for the choice $\Delta' = 3$ and $\beta = 0.52$.

5. – Numerical simulation of "limit cycles"

The "limit cycle" activity only occurs in plasma pulses presenting a large density or temperature gradient, giving rise to large diamagnetic velocities. For this reason we performed a series of simulations with eqs. (4) by assuming a large equilibrium density gradient. As in the benchmark attempt with low drift velocity, we chose a linear density profile providing a homogeneous drift velocity. However, we expected the island deformation to take place only in the nonlinear regime, when the partial flattening of the density profile inside the island separatrix would cause a diamagnetic velocity shear to occur across the separatrix. Unlike in the previous attempts, we did not have any reference in the literature to choose a set of parameters providing an island deformation comparable with the one observed in the experiments, so we had to increase progressively the parameters entering the diamagnetic drift velocity eq. (6) until a significant deformation of the island was reached.

We performed different simulations by varying two important parameters which determine the nonlinear island dynamics, that is Δ' and β, while keeping the others fixed: $L_n = 0.1$, $L_s = 1$, $\delta_i = 0.5$, $\eta = 0.001$. This choice turned out to be the best for exploring the parameter space, while trying to obtain a significant island deformation. The values for Δ' we chose for our different attempts come from the expression eq. (5), which holds for the magnetic equilibrium we chose in our simulations. In particular, the values $\Delta' = 3$, and $\Delta' = 5.3$ which we use below correspond to $L_y = 2$, and $L_y = 3$ respectively, where L_y is the half width of the integration box in the y-direction, and $k = 1/L_y$ is imposed. The β parameter is directly proportional to the diamagnetic drift frequency ω_{*i} and causes a reduction in the island growth rate. If the diamagnetic drift frequency is large enough, it causes a reversal in the island growth in the nonlinear phase. This is the kind of behavior we observed in our simulations. In fact, the hypothesis we wanted to test was that the diamagnetic effects cause the island deformation in the nonlinear regime, which in turn causes the cyclic activity, and the reversal of the island growth is a key feature of the "limit cycles".

Simulations performed on long time intervals show that the island, after the reduction phase, starts to grow again; then, after its size has increased enough, the growth inverts again and the island starts to decrease. This kind of behavior is consistent with the presence of a nonlinear stabilizing effect of the diamagnetic drift velocity, which causes a major deformation when the island width is larger. Every time the island experiences this reversal in its growth, the y-profile of ψ shows a significant component of the second harmonic, which is associated with an island deformation. This peculiar behavior is displayed in fig. 3, where two periods of this amplitude variation are shown.

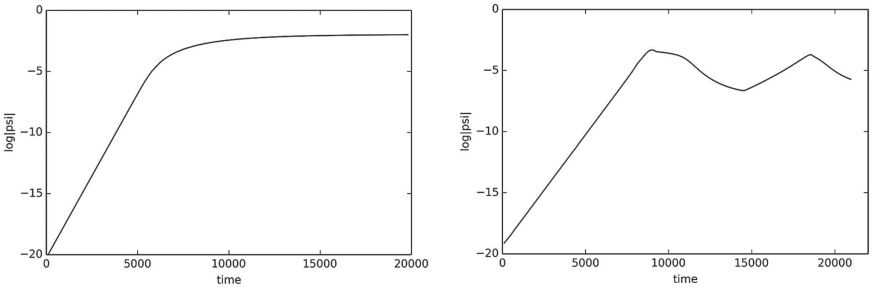

Fig. 4. – Logarithm of $|\psi|$ for the choice $\Delta' = 3$ and for two different values of β: on the left $\beta = 0.05$ and on the right $\beta = 0.52$.

For the sake of clarity, we show in fig. 4 the comparison between the $\log|\psi|$ for the choice $\Delta' = 3$ and for two different values of β. The left figure corresponds to $\beta = 0.05$ and the right figure corresponds to $\beta = 0.52$. In the first case the island width grows monotonically and tends to its saturation, while in the second case a reversal of the island growth occurs in the nonlinear regime.

To measure the island deformation, we chose to consider two indicators which are strictly related, namely the second y-derivative of ψ computed in the X-point on the resonant surface and the full width at half maximum (FWHM) of the same function. Also, we performed a Fourier analysis of the y-profile of ψ to see its harmonic content. In particular, we were interested in the relative weight of the second harmonic compared to the fundamental one. We show in fig. 5 the logarithm of $|\psi|$ (top left), the second derivative in the X-point (bottom left), the FWHM (top right) and the harmonic content

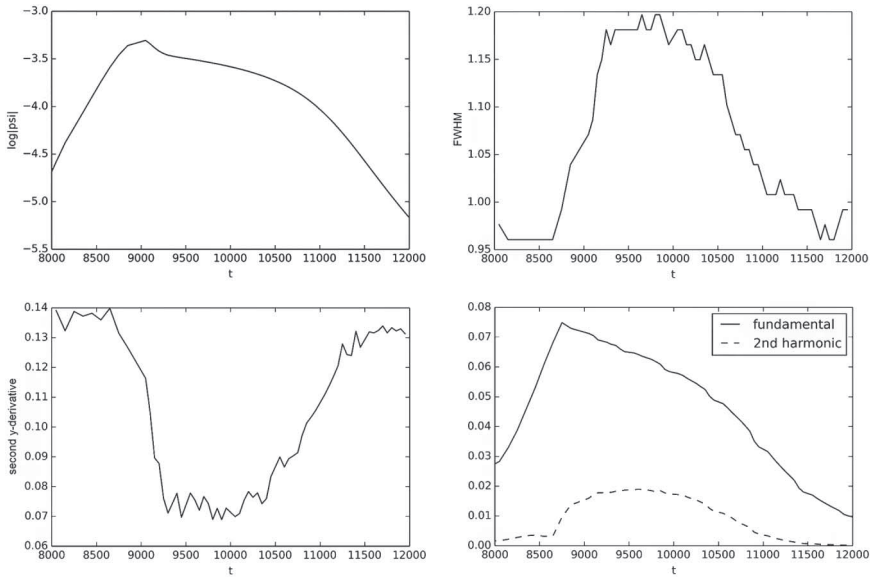

Fig. 5. – Logarithm of $|\psi|$ (top left), FWHM (top right), second derivative in the X-point (bottom left), harmonic content (bottom right) for the choice $\Delta' = 3$ and $\beta = 0.52$.

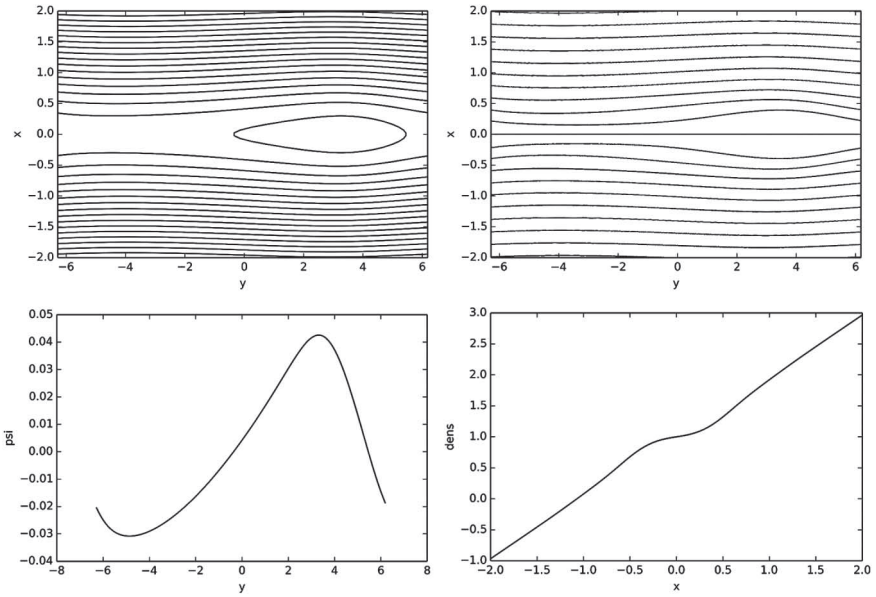

Fig. 6. – Contour plot of ψ (top left), contour plot of n (top right), y-profile of ψ (bottom left), density radial profile (bottom right) for the choice $\Delta' = 3$ and $\beta = 0.52$.

of the y-profile of ψ, fundamental and second harmonic (bottom right) for the choice $\Delta' = 3$ and $\beta = 0.52$. We display in this picture the zoom in the nonlinear phase across the first reversal of the growth to show the correlation between these indicators. The second derivative in the X-point is normalized to the full amplitude of the y-profile of ψ, so as to compensate for the increase in the amplitude, while the FWHM is normalized to the half-period of the equivalent sinusoidal wave, so that it is expected to be one when the signal is not distorted. These quantities are affected by the distortion of the signal, which corresponds to the large component of the second harmonic, in opposite ways: while the FWHM increases, the second derivative in the X-point decreases. Both the indicators provide a measure of the stretching of the X-point caused by the island deformation; however, the second y-derivative in the X-point is more affected by the peaking of the current profile which occurs in the large-Δ' regime, while the FWHM is not particularly affected by this phenomenon.

We display in fig. 6 the contour plots of the magnetic flux ψ and of the density n for the choice $\beta = 0.52$ to show the island deformation in the nonlinear regime and the fact that the density is a flux function. We also show in the same picture the shape of the corresponding y-profile of ψ and the density radial profile, which is partially flattened inside the separatrix. The field profiles have been taken at the reversal point of the island growth, where the island width reaches the maximum.

Attempts with lower values of Δ' did not show any significant deformation of the island. Attempts with even larger Δ' have been made to see whether larger island deformations could be obtained. We made a few simulations with the choice $\Delta' = 5.3$ and for different values of β. By increasing Δ' also the saturation width increases, and the diamagnetic effects in the nonlinear regime play a major role in the island deformation. On the other hand, the large Δ' also causes a significant current density peaking in the X-point when the island width grows above a threshold value [14]. This causes the

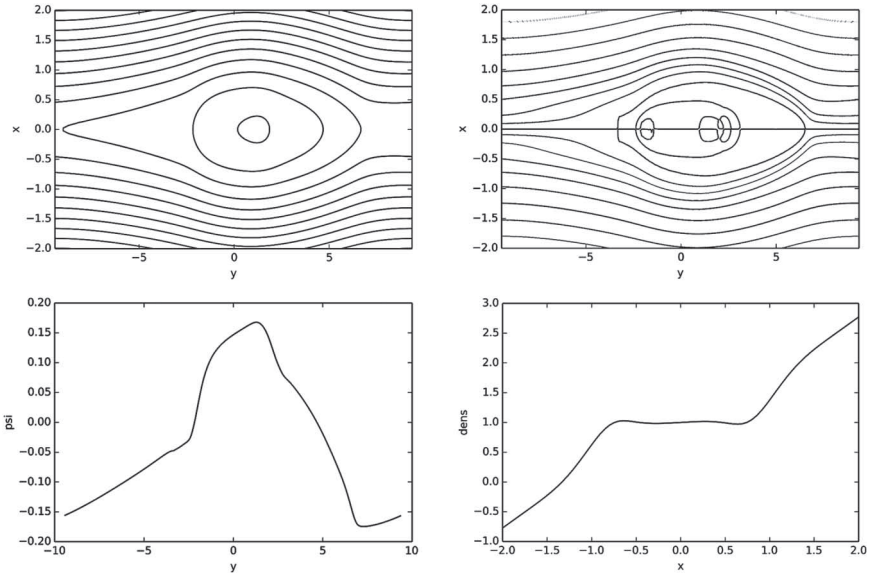

Fig. 7. – Contour plot of ψ (top left), contour plot of n (top right), y-profile of ψ (bottom left), density radial profile (bottom right) for the choice $\Delta' = 5.3$ and $\beta = 0.6$.

simulation to fail shortly after the island has reached the nonlinear regime, preventing any attempt to study the full-nonlinear behavior of the magnetic island in this regime of large Δ'. Also, the current peaking in the X-point compromises the validity of the second y-derivative of ψ as a deformation indicator, as mentioned above. We show in fig. 7 the field profiles taken at the reversal of the island growth, as in the previous attempts, for the choice $\Delta' = 5.3$ and $\beta = 0.6$. It is evident from this picture that the island deformation is much larger than before and the flattening of the density profile inside the separatrix is complete.

6. – Conclusions

In this paper we illustrated the attempts we have made to numerically simulate the phenomenon of "limit cycles", occurring in high-density pulses characterized by large density and temperature gradients in FTU. We performed several attempts with different values of the parameters entering our equations, namely Δ' and β, to understand the key factors which cause the onset of the "limit cycles". In particular, the attempt with $\Delta' = 3$ and $\beta = 0.52$ produced an amplitude evolution of the island which is in qualitative agreement with the one observed in the experiments during the cycle activity. The deformation of the y-profile of ψ at the reversal point of the island growth is supported by the two indicators we chose to calculate. Also, the presence of a large component of the second harmonic of the signal suggests that the island becomes significantly deformed when entering the nonlinear regime. The flattening of the density profile inside the separatrix suggests that the deformations may be caused by the shear in the diamagnetic drift velocity. If that is the case, the reversal in the growth is caused by the partial fragmentation of the island and not by a linear stabilization mechanism. To further support the hypothesis that this kind of dynamics causes the cycle activity, an accurate analysis of the mode frequency is necessary. We leave this task to a future work.

* * *

A. Casolari would like to express his gratitude to Paolo Buratti from ENEA, Frascati for the consultancy during the writing of this paper and Francesco Pegoraro from Università di Pisa for the valuable discussions. He also wants to acknowledge Daniela Grasso from CNR and Politecnico di Torino for lending him the code which was used to perform the simulations and for helping him in the acquisition and the interpretation of the numerical results.

REFERENCES

[1] Furth H. P., Killeen J. and Rosenbluth M. N., *Phys. Fluids (1958–1988)*, **6** (1963) 459.
[2] Rutherford P. H., *Phys. Fluids*, **16** (1973) 1903.
[3] Ara G., Basu B., Coppi B., Laval G., Rosenbluth M. N. and Waddell B. V., *Ann. Phys. (N.Y.)*, **112** (1978) 443.
[4] Grasso D., Ottaviani M. and Porcelli F., *Nucl. Fusion*, **42** (2002) 1067.
[5] Pucella G., Buratti P., Cianfarani C., Giovannozzi E. and FTU team, *Proceedings of the 42nd EPS Conference on Plasma Physics (Lisbon, Portugal, 22–26 June 2015)*, in *ECA*, Vol. **39E** (European Physical Society) 2015, P4.112 (`http://ocs.ciemat.es/EPS2015PAP/pdf/P4.112.pdf`).
[6] Pucella G., Tudisco O., Apicella M. L., Apruzzese G., Artaserse G., Belli F., Bin W., Boncagni L., Botrugno A., Buratti P. *et al.*, *Nucl. Fusion*, **53** (2013) 083002.
[7] Pegoraro F. and Schep T. J., *Plasma Phys. Controll. Fusion*, **28** (1986) 647.
[8] Ottaviani M., Porcelli F. and Grasso D., *Phys. Rev. Lett.*, **93** (2004) 075001.
[9] Scott B. D., Hassam A. B. and Drake J. F., *Phys. Fluids (1958–1988)*, **28** (1985) 275.
[10] Hazeltine R. D., Kotschenreuther M. and Morrison P. J., *Phys. Fluids*, **28** (1985) 2466.
[11] Harris E. G., *Il Nuovo Cimento (1955–1965)*, **23** (1962) 115.
[12] White R. B., Monticello D. A., Rosenbluth M. N. and Waddell B. V., *Phys. Fluids (1958–1988)*, **20** (1977) 800.
[13] Grasso D., Borgogno D. and Tassi E., *Commun. Nonlinear Sci. Numer. Simul.*, **17** (2012) 2085.
[14] Ali A., Li J. and Kishimoto I., *Phys. Plasmas (1994–present)*, **21** (2014) 052312.